

Group-IV Pentaoctite: A New 2D Material Family

Vanessa D. Kegler^{1,2,*}, Igor S. S. de Oliveira^{3,†}, Dominike Pacine^{4,‡},
Ricardo W. Nunes^{5,§}, Teldo A. S. Pereira^{1,6,¶} and Erika N. Lima^{1,6,**}

¹Physics Graduate Program, Institute of Physics,
Federal University of Mato Grosso, Cuiabá, MT, Brazil

²Physics Department, Federal University of Rondônia, Campus Ji-Paraná, Ji-Paraná, RO, Brazil

³Physics Department, Federal University of Lavras, Lavras, MG, Brazil

⁴Federal Institute of Education, Science and Technology of Triângulo Mineiro, Uberlândia, MG, Brazil

⁵Physics Department, Federal University of Minas Gerais, Belo Horizonte, MG, Brazil

⁶National Institute of Science and Technology on Materials Informatics, Campinas, Brazil
(Dated: September 13, 2024)

This study investigates the structural, mechanical, and electronic properties of novel two-dimensional (2D) pentaoctite (PO) monolayers composed of group-IV elements (PO-C, PO-Si, PO-Ge, and PO-Sn) using first-principles calculations. Stability is explored through phonon spectra and ab initio molecular dynamics simulations, confirming that all proposed structures are dynamically and thermally stable. Mechanical analysis shows that PO-C monolayers exhibit exceptional rigidity, while the others demonstrate greater flexibility, making them suitable for applications in foldable materials. The electronic properties show semimetallic behavior for PO-C and metallic behavior for PO-Si, while PO-Ge and PO-Sn possess narrow band gaps, positioning them as promising candidates for semiconductor applications. Additionally, PO-C exhibits potential as an efficient catalyst for the hydrogen evolution reaction (HER), with strain engineering further enhancing its catalytic performance. These findings suggest a wide range of technological applications, from nanoelectronics and nanomechanics to metal-free catalysis in sustainable energy production.

I. INTRODUCTION

Since the first demonstration of atomically thin two-dimensional (2D) systems, which led to the discovery of graphene through micromechanical cleavage,^[1–3] many other 2D materials with structures similar to graphene have been extensively explored in the literature.^[4] In particular, structures composed of group-IV elements, such as silicene,^[5, 6] germanene,^[5, 7] and stanene,^[8, 9] have been theoretically predicted and subsequently synthesized. These materials exhibit properties distinct from graphene, such as topologically nontrivial electronic states.^[10, 11] Moreover, the presence of a band gap in these materials can overcome graphene's limitations for applications that require a finite band gap, such as the fabrication of field-effect transistors.^[12]

Numerous 2D planar graphene allotropes composed of carbon atoms have been proposed. Among these, graphyne and graphdiyne, which stand out as two well-studied structures, exhibit unique properties due to acetylenic linkages (consisting of single and triple bonds) between carbon atoms.^[13, 14] Biphenylene, a planar carbon structure composed of octagonal, hexagonal, and square arrangements of atoms, has recently been synthesized.^[15] Several other graphene allotropes have been identified, each with distinct features.^[16, 17] These materials possess exceptional electronic and mechanical properties, making them highly relevant for various scientific and technological applications, such as nanoelectronics, energy storage, and biosensors.^[18–20]

Another approach to modifying graphene properties is by introducing extended defects along its structure. For instance, the 558 line defect comprises octagonal

and pentagonal sp^2 -hybridized carbon rings integrated within a pristine graphene lattice.^[21] Moreover, many other defects have been introduced along the graphene structure.^[22] These defects can be utilized to tailor the properties of graphene, expanding its range of potential applications.

In Ref. 23, the authors propose two new 2D carbon allotropes composed of octagonal and pentagonal carbon rings, demonstrating through first-principles simulations that these structures are energetically and dynamically stable. One structure features a linear arrangement of 558-membered carbon rings, while the other exhibits a zigzag configuration of the same rings. The 558 zigzag configuration has also been shown to form a bismuth 2D sheet, referred to as pentaoctite Bi,^[24, 25] which exhibits topological insulator behavior. Moreover, a new 2D pentaoctite phase in group-V nanostructures, i.e., allotropes of phosphorene, arsenene, and antimonene, has been theoretically investigated.^[26] The study reveals that these structures are stable, exhibit tunable band gaps, and hold potential applications in optoelectronics due to their absorption in the visible spectrum.

Here, we employ first-principles calculations to explore 2D materials and predict that, in addition to carbon, other group-IV elements (namely silicon, germanium, and tin) can also adopt the pentaoctite structure. We present a detailed investigation of the structural, mechanical, and electronic properties of group-IV pentaoctite sheets. Additionally, we investigate the catalytic activity of the carbon pentaoctite (PO-C) structure in the hydrogen evolution reaction (HER).

II. COMPUTATIONAL DETAILS

Our first-principles calculations are based on the Density Functional Theory (DFT),[27, 28] as implemented in the Vienna Ab initio Simulation Package, VASP.[29] The generalized gradient approximation (GGA) describes the exchange and correlation potentials as parametrized by Perdew, Burke, and Ernzerhof (PBE).[30] The interactions between the valence electrons and the ionic cores are treated using the projector augmented wave (PAW) method.[31, 32] The electronic wave functions are expanded on a plane-wave basis with an energy cutoff of 500 eV. The supercells are on the xy -plane and the Brillouin zone integrations are performed using a $10 \times 10 \times 1$ Γ -centered Monkhorst-Pack sampling.[33] To avoid interactions between the periodic images of the supercell, the systems are modeled using supercells repeated periodically on the xy -plane with a vacuum region of about 20 Å along the z -direction. The cell parameters and ionic positions are fully optimized until the residual force on each atom is less than 0.01 eV/Å. Phonon properties were calculated using the Density Functional Perturbation Theory (DFPT) method, as implemented in the PHONOPY code.[34] The thermal stability was verified by *Ab Initio* Molecular dynamics (AIMD) simulations using the Andersen thermostat.[35] The elastic constants, C_{ij} , were calculated based on the stress-strain method implemented in the VASPKIT code.[36] In the electronic structure calculations, we used the Hyded-Scuseria-Enzerhof (HSE06) hybrid functional[37] to avoid underestimating the band gap value of the group-IV pentaoctite monolayers. The screened parameter was set to 0.2 Å⁻¹, and 25% of the screened Hartree-Fock (HF) exchange was mixed with the PBE exchange functional in the HSE06 method. Additionally, all electronic structure calculations include spin-orbit coupling (SOC).

III. RESULTS AND DISCUSSION

A. Structural properties and stabilities

The pentaoctite (PO) monolayers composed by elements from the group-IV (PO-IV, for IV = C, Si, Ge, and Sn) crystallize in the orthorhombic symmetry with 12 atoms in the unit cell, as shown in the structural models in Fig.1. The top views reveal that these new 2D allotropes are composed of two side-sharing pentagons connected to an octagon. The bond lengths vary from 1.39–1.48 Å for PO-C, 2.24–2.31 Å for PO-Si, 2.44–2.53 Å for PO-Ge, and 2.83–2.92 Å for PO-Sn monolayers. The side view in Fig.1(a) reveals that the PO-C sheet presents a planar structure similar to graphene. On the other hand, the remaining structures present a buckled construction [see Figs.1(b),1(c) and 1(d)], which is similar to their group-IV graphene-like counterparts,[5, 8] and also to group-V pentaoctite.[26] It is worth mentioning that PO-Si shows a simple two-layered atomic

structure, while PO-Ge and PO-Sn have a more complex three-layered structure. It occurs because the buckling height (h) follows the increases in the atomic radius of group-IV. The optimized structural parameters and bond lengths of the PO-IV structures are presented in Table I.

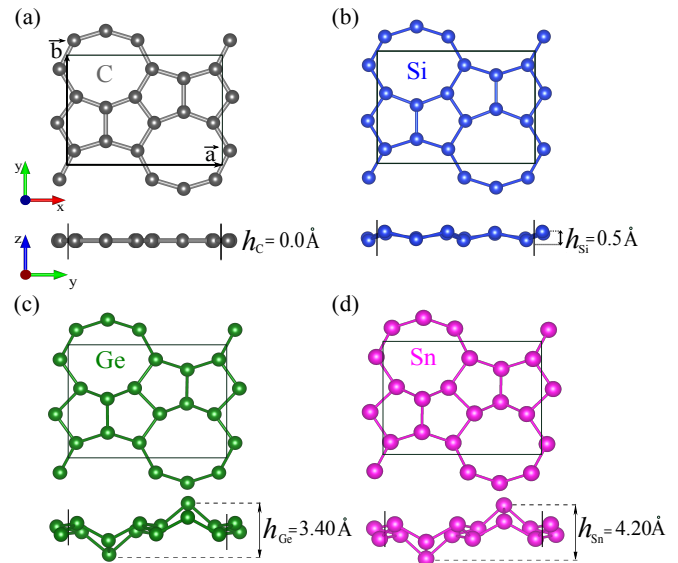


FIG. 1. Top and side views of the crystal structures of the (a) PO-C, (b) PO-Si, (c) PO-Ge, and (d) PO-Sn monolayers. The primitive cell containing 12 atoms is marked in the black rectangular area with solid lines defined by the lattice vectors \vec{a} and \vec{b} . h_C , h_{Si} , h_{Ge} and h_{Sn} represent the buckling height for PO-C, PO-Si, PO-Ge, and PO-Sn monolayers. The grey, blue, green, and magenta balls represent the C, Si, Ge, and Sn atoms.

TABLE I. Optimized structural parameters of PO-IV monolayers, including lattice constants (a and b), buckling height (h), and bond length ranges.

Structure	a (Å)	b (Å)	h (Å)	Bond length range (Å)
PO-C	6.9	4.87	0.00	1.39–1.48
PO-Si	10.81	7.68	0.51	2.24–2.31
PO-Ge	10.56	7.86	3.40	2.44–2.53
PO-Sn	11.85	8.98	4.20	2.83–2.92

Fig.2 (a)-(d) shows the phonon dispersion of the PO-IV monolayers. No imaginary frequencies are observed within the first Brillouin zone, indicating its dynamical stability. Moreover, near the Γ point of the Brillouin zone, the lowest frequency mode (ZA) exhibits quadratic dispersion. In contrast, the two other modes, longitudinal acoustic (LA) and transverse acoustic branches (TA), display a linear dependence on the wave vector, which is characteristic of 2D materials. Then, we check the structural stability of these PO-IV monolayers at room temperature through *ab initio* molecular dynamics (AIMD) simulations. Fig.3 (a)-(d) displays the potential energy

fluctuations (ΔE) during the simulation time, along with a crystal structure snapshot of the last configuration at 15 ps. All structures maintain their integrity at temperatures up to 300 K, demonstrating good thermal stability at room temperature.

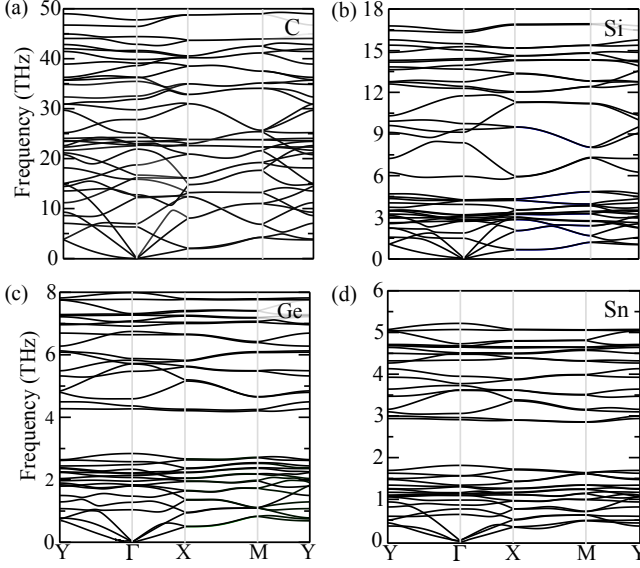


FIG. 2. Phonon dispersion relations of the (a) PO-C, (b) PO-Si, (c) PO-Ge, and (d) PO-Sn monolayers.

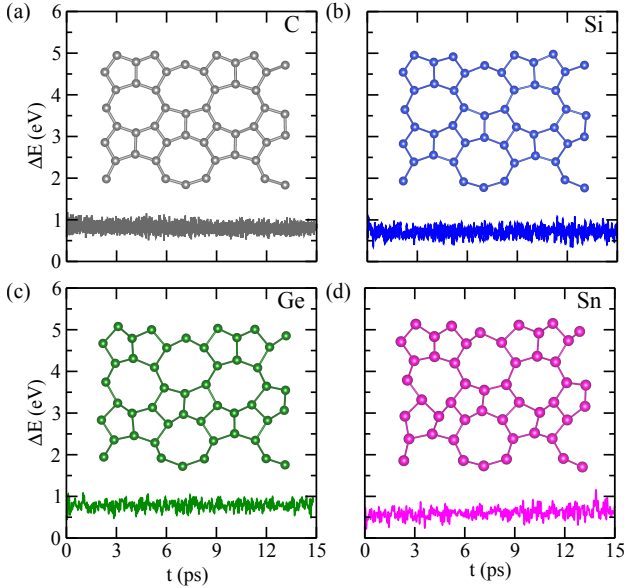


FIG. 3. Potential energy fluctuation profiles during AIMD simulations at 300 K for the (a) PO-C, (b) PO-Si, (c) PO-Ge, and (d) PO-Sn monolayers. The snapshots of the crystal structures at 15 ps for the monolayers are shown in the insets.

We also verified the energetic stability of these 2D allotropes by calculating their formation energy (E_F) relative to their corresponding hexagonal structures. To

compute the (E_F), we used the equation $E_F = E_{PO} - E_{hex}$, where E_{PO} represents the energy per atom in a PO structure and E_{hex} represents the energy per atom in a hexagonal structure. The calculated relative formation energies for C, Si, Ge, and Sn structures are 350, 120, 90, and 60 meV/atom. These results confirm that the PO-IV structure is energetically metastable compared to its previously synthesized hexagonal counterparts.[2, 38, 39] Furthermore, when we compared these values with another previously synthesized carbon allotrope, biphenylene ($E_F = 470$ meV/atom),[40] it is clear that this new 2D allotrope of group-IV has significant potential for experimental realization.

B. Mechanical properties

From the above indications that the PO-IV is metastable, we proceeded to analyze its mechanical stability. The elastic constants C_{11} , C_{22} , $C_{12} = C_{21}$, and C_{66} and the mechanical properties of this new 2D rectangular lattice allotrope are listed in Table II, together with the values obtained from hexagonal structures. The elastic constants satisfy the Born-Huang criterion:[41, 42] $C_{11}C_{12} - C_{12}^2 > 0$ and $C_{66} > 0$, suggesting that PO-IV sheets are mechanically stable to resist small deformations.

Our results indicate a decrease in Young's modulus (E_{max}) of PO-IV structures from C to Sn (333.01 – 13.60 N/m), following the same tendency observed in hexagonal phases (344.01 – 24.46 N/m). This trend in Young's modulus directly results from the transition from strong covalent bonding in small atoms (C) to weaker metallic bonding in larger atoms (Sn). The decrease in bond strength as we move down the group-IV elements is a crucial factor in the stiffness of the materials, leading to a lower Young's modulus. The elastic moduli values of the PO-C monolayer are $E_x = 333.01$ N/m and $E_y = 254.50$ N/m. It is important to note that in the x -direction, Young's modulus of PO-C is only 3.31% lower than that of graphene (344.41 N/m).[43] Furthermore, compared to biphenylene, which has Young's moduli of $E_x = 259.7$ N/m and $E_y = 212.4$ N/m,[45] PO-C exhibits a 27.45% larger modulus in the x -direction and 19.82% larger along the y -direction. These findings suggest that PO-C is highly robust, making it an ideal material for nanomechanical applications due to its exceptional intrinsic strength.

The elastic moduli of Si ($E_x = 56.61$ N/m, $E_y = 42.40$ N/m), Ge ($E_x = 8.26$ N/m, $E_y = 27.28$ N/m), and Sn ($E_x = 5.81$ N/m, $E_y = 13.60$ N/m) sheets are also smaller than those of their respective hexagonal phases, as listed in Table II, as well as other well-known 2D materials, such as MoS₂ (120 N/m)[46] and black phosphorus ($E_x = 22$ N/m, $E_y = 56$ N/m).[47] Thus, we can infer that Si, Ge, and Sn structures hold great potential for applications in folding materials.

TABLE II. Elastic constants (C_{11} , C_{12} , C_{22} , C_{66}), Young's modulus (E_x , E_y , E_{max}), and Poisson's ratio (ν_x , ν_y , ν_{max}) of the PO-IV monolayers. The elastic constants and Young's modulus are given in units of N/m, while Poisson's ratio is dimensionless.

Structure	C_{11}	C_{22}	C_{12}	C_{66}	E_x	E_y	E_{max}	ν_x	ν_y	ν_{max}	Reference
PO-C	270.21	345.22	65.14	100.61	333.01	254.50	333.01	0.19	0.24	0.29	This work
Graphene	354.12	354.12	58.65	142.38	344.41	344.41	344.01	0.17	0.17	0.17	[43]
PO-Si	65.95	47.52	17.96	16.54	56.61	42.40	56.61	0.38	0.28	0.38	This work
Silicene	-	-	-	-	61.33	61.33	61.33	0.32	0.32	0.32	[44]
PO-Ge	8.50	28.09	2.61	4.66	8.26	27.28	27.28	0.09	0.31	0.31	This work
Germanene	-	-	-	-	42.05	42.05	42.05	0.33	0.33	0.33	[44]
PO-Sn	5.82	14.04	1.23	0.87	5.81	13.60	13.60	0.10	0.20	0.70	This work
Stanene	-	-	-	-	24.46	24.46	24.46	0.39	0.39	0.39	[44]

$$E(\theta) = \frac{X}{C_1 a^2 + [X/C_{66} - 2C_{12}]ab + C_{22}b^2}, \quad (1)$$

$$\nu(\theta) = \frac{C_{12}a^2 - [C_{11} + C_{22} - X/C_{66}]ab + C_{12}b^2}{C_1 a^2 + [X/C_{66} - 2C_{12}]ab + C_{22}b^2}, \quad (2)$$

where $a = \sin^2(\theta)$, $b = \cos^2(\theta)$, and $X = C_{11}C_{22} - C_{12}^2$. According to the diagrams in Fig.4, Young's modulus and Poisson's ratio exhibit strong anisotropy across all PO-IV structures, with the effect being more pronounced in the PO-Ge [fig.4(c)] and PO-Sn [fig.4(d)] monolayers. For PO-C and PO-Si, the maximum values of Young's modulus (333.01 and 56.61 N/m) occur at $\theta = 0^\circ$, and the minimum values (254.50 and 42.40 N/m) at $\theta = 90^\circ$. In contrast, Young's modulus of PO-Ge reaches its maximum value at $\theta = 90^\circ$ (27.28 N/m) and its minimum value (8.26 N/m) at $\theta = 0^\circ$, while PO-Sn reaches its maximum value (13.60 N/m) at $\theta = 90^\circ$ and its minimum value (5.81 N/m) at $\theta = 45^\circ$.

Regarding Poisson's ratio values, PO-IV sheets have proven to be exceptionally versatile materials. Based on the polar plot of Poisson's ratio, the most anisotropic structure in this category is the PO-Sn [Fig.4 (d)], with a maximum Poisson's ratio of 0.70, which is 7 times greater than the minimum value of 0.10. Next, PO-Ge [Fig.4 (d)] shows a ratio of almost 3.5. Lastly, PO-C [Fig.4 (a)] and PO-Si [fig.4 (b)] are the less anisotropic structures, with ratio values of 1.53 and 1.36, respectively. Our results show that the maximum values of Poisson's ratio of PO-IV are higher than those of their respective hexagonal phases, except for PO-Ge, see Table II. Thus, we conclude that the anisotropy of the pentaoctite structures makes them potential candidates for designing new devices with tailored mechanical properties for advanced technological applications.

C. Electronic properties

Fig.5 shows the orbital-projected electronic band structures and density of states (DOS) of the PO-IV monolayers. The inset in Fig.5(a) illustrates the direction along the high symmetry points used to calculate the electronic band structure. PO-C exhibits a tilted

Dirac cone at the Fermi level along the Γ -Y direction, as illustrated in Fig.5(a). Additionally, the DOS at the Fermi level provides evidence of the presence of a Dirac cone. Unlike PO-C, which presents semimetallic features, PO-Si is a metal [Fig.5(b)], showing a hole pocket along the M-X direction. Furthermore, as shown in Figs.5(c) and 5(d), PO-Ge and PO-Sn monolayers present a direct band gap along the Γ -Y direction, with band gap values of 45 and 111 meV, respectively. Notably, the band gaps of PO-IV monolayers closely resemble those of their corresponding hexagonal phases: graphene (metal), silicene (1.55 meV), germanene (33 meV), and stanene (100 meV). [2, 6, 7, 48] Moreover, methods such as chemical functionalization, the application of external electric fields, and strain engineering offer additional pathways to optimize their optical and electronic behavior, positioning these materials at the forefront of 2D materials research.

In general, the projections of the p_z orbitals (red balls) dominate the states at the Fermi level for all studied PO-IV monolayers. For PO-C, the orbital projections indicate that most of the contribution comes from p_z orbitals, while p_x and p_y orbitals exhibit more relevant contributions at deeper energy levels (not shown). The significant presence of p_z states around the Fermi level is characteristic of 2D carbon-based systems like graphene and biphenylene. This prevalence of p_z orbitals not only suggests the potential for constructing van der Waals heterostructures but also indicates reactivity favorable for adsorption processes, making these materials highly applicable in nanoelectronics and sensor devices. For the other structures, there is a noticeable reduction in the p_z states, while the p_y states become more prominent, as illustrated in Figs.5(b), 5(c) and 5(d).

The influence of p_z orbitals on the structural stability of single-layer materials is significant due to their role in π -bonding. For instance, in graphene, p_z orbitals form a delocalized π -conjugated system, leading to a stable, flat structure.[3] However, in silicene, the larger and more diffuse p_z orbitals of silicon atoms reduce the effective overlap and weaken π -conjugation. This leads to a buckled structure that minimizes energy through enhanced σ -bonding stabilization.[49]

To understand better the results observed in the orbital

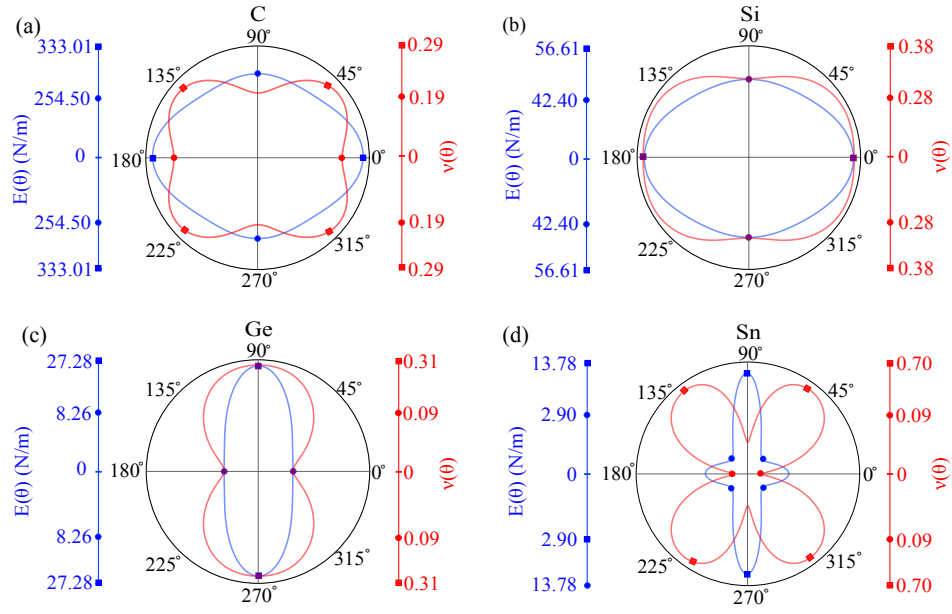


FIG. 4. Polar plots illustrating the directional dependence of Young's modulus and Poisson's ratio of the (a) PO-C, (b) PO-Si, (c) PO-Ge, and (d) PO-Sn monolayers. The squares (circles) indicate the maximum (minimum) values of $E(\theta)$ (blue symbols) and $\nu(\theta)$ (red symbols).

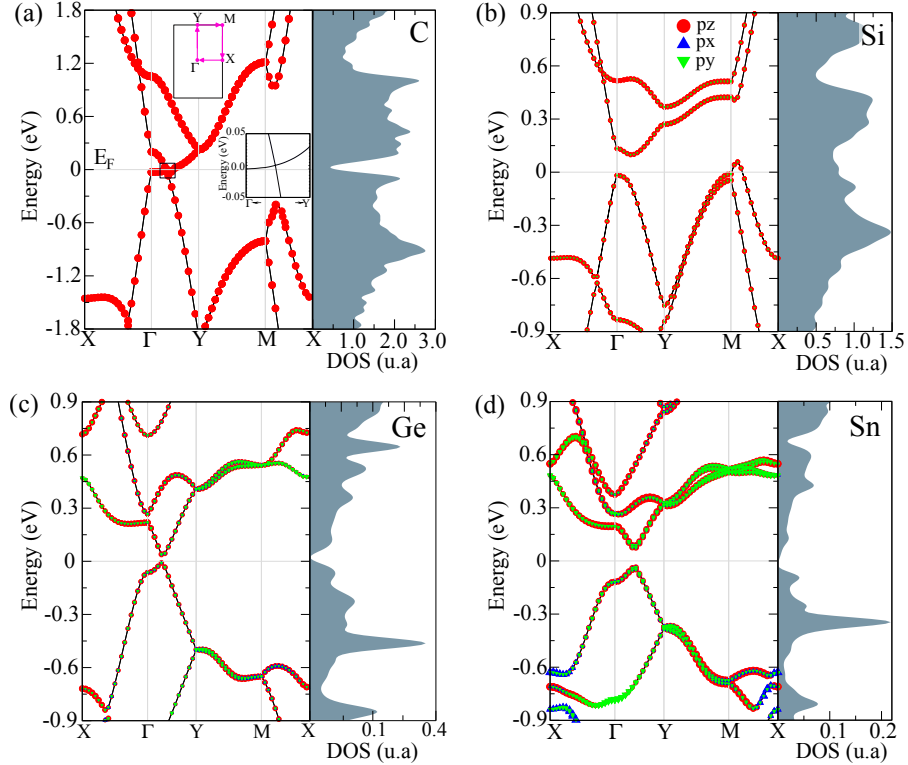


FIG. 5. Orbital-projected electronic band structures and density of states (DOS) of the (a) PO-C, (b) PO-Si, (c) PO-Ge, and (d) PO-Sn monolayers. The red (balls), blue (triangles up), and green (triangles down) symbols represent the s, p, and d orbitals contributions. The size of the symbols shows the relative contribution from the orbitals.

projections depicted at the band structures, we also analyzed the charge density of the lowest unoccupied states

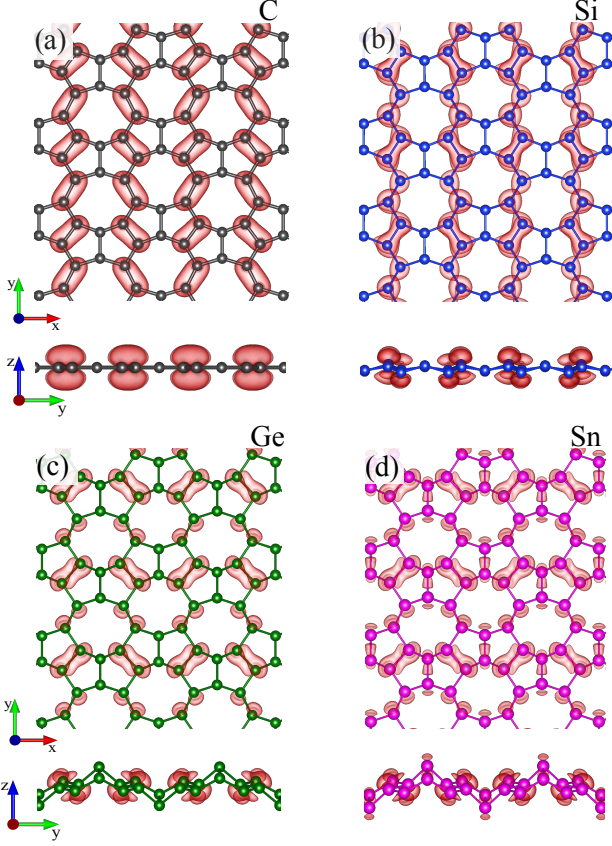


FIG. 6. Top and front views of the partial charge density at $E - E_F \approx 100$ meV of the (a) PO-C, (b) PO-Si, (c) PO-Ge, and (d) PO-Sn monolayers. Isosurface value is set $10^{-4} e/\text{\AA}^3$.

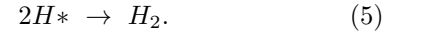
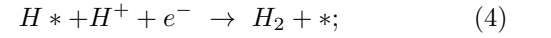
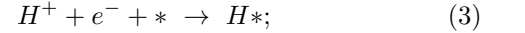
around $E - E_F \approx 100$ meV, shown in Fig. 6. In the PO-C sheet [Fig. 6(a)], there is an extensive overlap of p_z orbitals similar to the π -delocalized states observed in graphene. Meanwhile, Si, Ge, and Sn monolayers depicted in Figs. 6(b), 6(c) and 6(d) show a less effective and more diffuse overlap of p_z orbitals, similar to what is observed in silicene, germanene, and stanene.[48–50]

The predominance of p_z orbitals in the PO-C monolayer suggests a structural trend similar to graphene, resulting in a perfectly flat structure, as depicted in Fig. 1 (a). On the other hand, the larger covalent radii of Si (1.11 Å), Ge (1.20 Å), and Sn (1.39 Å) atoms compared to C (0.76 Å) atom directly influence the p_z orbital overlap, leading to reduced π -conjugation and a natural preference for a buckled structure. Furthermore, the effective overlap of p_y and p_z orbitals in these materials strongly enhances the structural buckling and stabilizes the system. As a result, in comparison to germanene[50], which exhibits a mix of sp^2 and sp^3 hybridization within its buckled structure, our studied Si, Ge, and Sn sheets also display both sp^2 and sp^3 hybridization bonding. This behavior underscores the importance of p_z orbitals in influencing the structural and electronic characteristics of PO-IV structures.

D. PO-C HER performance

As fossil fuel reserves decrease and the resulting environmental threats become more pressing, the development and use of clean, sustainable energy sources are rapidly accelerating. In this growing field of renewable options, hydrogen (H_2) emerges as a strong candidate for building a sustainable future.[51] Recognized for its safety, absence of pollutants, effective utilization, and substantial energy yield, hydrogen carries significant promise in fueling our societal needs. Exploring the viability of hydrogen storage has emerged as a prominent subject across the scientific community.[52] Nevertheless, the inherently low intermolecular forces of H_2 molecules hinder their effective packing, creating challenges for storing H under ambient conditions.[53] A very well-explored route to produce H_2 is through the hydrogen evolution reaction (HER),[54] which typically occurs at the surface of a metallic catalyst. 2D materials have been extensively investigated in the last few years as promising catalysts for HER.[55, 56] In this context, we investigated the catalytic activity of the metallic PO-C structure.

To investigate the HER performance of the PO-C structure, we consider the systems in acidic media, where the reaction path of HER can be described by the following steps:



Eq. 3 is a reduction of a proton (H^+) on an active site ($*$) of the substrate (Volmer step), Eqs. 4 and 5 show the evolution of molecular H_2 through a second H^+/e^- transfer (Heyrovsky step) or by the combination of two adsorbed H (Tafel step), respectively. The variation in the Gibbs free energy for the H adsorption (ΔG_{H^*}) is given by

$$\Delta G_{H^*} = \Delta E_H + \Delta E_{ZPE} - T\Delta S_H, \quad (6)$$

where ΔS_H represents the entropy change from before to after H adsorption at $T = 298.15$ K, ΔE_{ZPE} is the zero-point energy difference between adsorbed H and the gas phase (H_2), and $\Delta E_H = E_{\text{sub}+H} - E_{\text{sub}} - \frac{1}{2}E_{H_2}$ describes the adsorption energy of H^* , with $E_{\text{sub}+H}$, E_{sub} and H_2 represents the total energy of the substrate with adsorbed H, pristine substrate, and H_2 molecule, respectively. The ΔE_{ZPE} and $T\Delta S_H$ terms are nearly independent of the catalysts;[57, 58] therefore, we use the values described in Ref. 57, which have been employed in other studies of HER on 2D materials.[59–63] Following this procedure, Eq. 6 can be written as $\Delta G_{H^*} = \Delta E_H + 0.24$ eV.

In Fig. 7(a), we present ΔG_{H^*} values for hydrogenated PO-C at three different deposition sites, represented in Fig. 7(b). For benchmark purposes, we also consider the graphene structure and obtain $\Delta G_{H^*} = 1.68$ eV, which

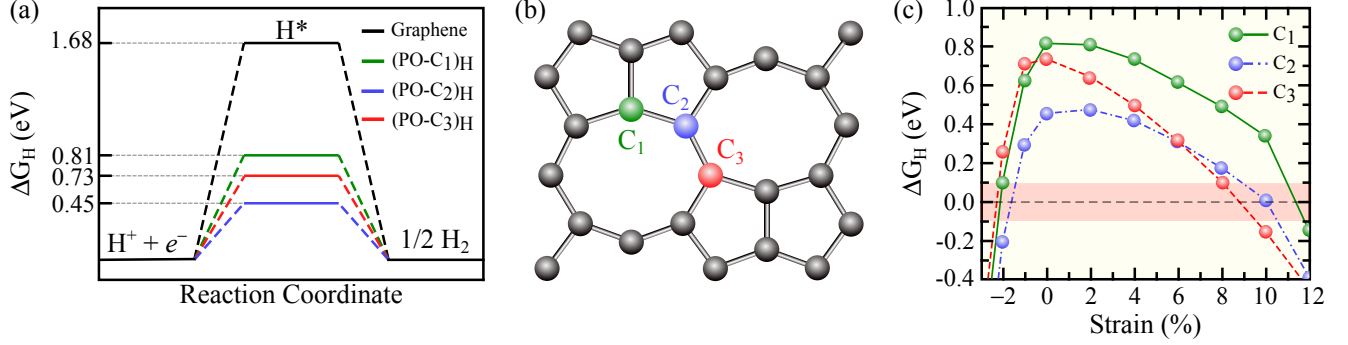


FIG. 7. (a) Gibbs free energy (ΔG_{H^*}) for hydrogen adsorption at the C₁, C₂, C₃ sites, represented in (b). ΔG_{H^*} for graphene is also included. (c) ΔG_{H^*} values of the C₁, C₂, and C₃ configurations under biaxial strain conditions. The red region in (c) indicates values where $|\Delta G_{H^*}| \leq 0.1$ eV. The colors green, blue, and red refer to C₁, C₂, and C₃ sites, respectively.

aligns closely with the 1.66 eV value reported in Ref.[64]. With the definitions used, $\Delta G_{H^*} \rightarrow 0$ characterizes an ideal catalyst. Therefore, H adsorbed on the PO-C₂ site [(PO-C₂)_H] exhibits the highest catalytic activity, with $\Delta G_{H^*} = 0.45$ eV. The results indicate an energy difference of approximately 44% for PO-C between C sites 1 and 2, with an intermediate value at C₃. Positive values suggest that the process of H adsorption onto the catalyst is energetically unfavorable from a kinetic standpoint; as a consequence, the PO-C structure has a higher catalytic efficiency than pristine graphene. Although it presents a lower catalytic property than biphenylene.[45] It has been shown that in non-hexagonal rings, the strain caused by deviation from the ideal value of 120° in the sp^2 hybridization and antiaromaticity enhances the HER catalytic activity.[65] Moreover, as it has been shown for other 2D structures, the PO-C performance might be enhanced through atomic defects or doping.[66–68]

The HER performance can be tuned by applying strain, which has proven to be a highly effective strategy for altering the reactivity of metal catalysts.[68] We show that applying strain to the PO-C structure allows for tuning its ΔG_{H^*} values, as presented in Fig. 7(c). We observe a decrease in ΔG_{H^*} as the strain increases in all three analyzed cases. For (PO-C₁)_H, (PO-C₂)_H, and (PO-C₃)_H systems, at stretching levels of 11.34%, 10%, and 8.75%, respectively, we find $\Delta G_{H^*} \rightarrow 0$ eV which is comparable to the catalytic properties of a Pt surface.[57]. A compressive strain of -2%, -1.54%, and -2.25% for the (PO-C₁)_H, (PO-C₂)_H, and (PO-C₃)_H, respectively, also results in $\Delta G_{H^*} \rightarrow 0$ eV. Notably, both the C₂ and C₃ sites demonstrate high catalytic activity under tensile strains of 9.1% to 9.54%, with $\Delta G_{H^*} < 0.1$ eV, as shown in the red region of Fig. 7(c). Similar activity is also observed for C₁ and C₃ sites under a compressive strain of -1.8%. This indicates that, at specific strain values, the surface of the PO-C monolayer can have up to 66.6% of their sites catalytically active for HER with $|\Delta G_{H^*}| \leq 0.1$ eV.

Our findings reveal that strain engineering markedly enhances the hydrogen evolution reaction (HER) activity in PO-C sheets. Applying strain results in the creation of active sites with hydrogen adsorption energies ($|\Delta G|$) ranging from 0 to 0.1 eV, which are comparable to those of platinum (Pt)-based metallic catalysts.[69–71] However, it is important to note that Pt-based catalysts suffer from issues like limited availability and poor stability.[72, 73] In addition, substituting Pt-based materials with alternative materials can significantly reduce the cost of the catalyst.[73] These findings demonstrate that strain engineering is a versatile and effective approach for optimizing the catalytic activity of the PO-C structure, offering a tunable method to enhance HER performance. Thus, our results strongly suggest that the PO-C monolayer holds great potential as a metal-free catalyst for HER.

IV. CONCLUSION

In summary, we investigated the structural, electronic, and mechanical properties of the 2D allotrope of group-IV elements (C, Si, Ge, and Sn) called pentaoctite. Our findings reveal that in the x -direction, the PO-C monolayer is as rigid as graphene, while PO-Si, PO-Ge, and PO-Sn are more flexible than their hexagonal counterparts, which suggests a possible application for these sheets in foldable materials. Additionally, the 2D representation of Young's modulus and Poisson's ratio indicates that this new 2D allotrope exhibits highly anisotropic mechanical properties.

The electronic band structure calculations reveal that PO-Ge and PO-Sn sheets are direct band gap semiconductors with values of 45 and 111 meV, while PO-Si and PO-C exhibit metallic properties with distinct electronic characteristics. Specifically, PO-Si is characterized by a valence band crossing the Fermi level, whereas PO-C features a tilted Dirac cone at the Fermi level. The unique

metallic properties of PO-C make it a promising candidate to be a catalyst for HER. The Gibbs free energy analysis demonstrates that under strain conditions, the PO-C sheet performs comparably to the best catalysts for HER found in the literature, e.g., the Pt-surface, with $\Delta G_{H^*} \rightarrow 0$ eV.

Our findings indicate that the PO-IV monolayer is well-suited for nanoelectronics and nanomechanics, with PO-C, in particular, also serving as a metal-free electrocatalyst for HER. Additionally, PO-IV sheets show strong potential for experimental realization.

ACKNOWLEDGMENTS

The authors acknowledge financial support from INCT-Materials Informatics and computer time from CENAPAD-UNICAMP and the Brazilian National Scientific Computing Laboratory (LNCC). I.S.S.d.O. acknowledges financial support from FAPEMIG (Project No. APQ-01425-21) and computer time from LCC-UFLA. T.A.S.P acknowledges PDPG-FAPDF-CAPES Centro-Oeste grant number 00193-00000867/2024-94 and support from CNPq grants 408144/2022-0 and 423423/2021-5. E.N.L. thanks to Augusto de Lelis Araújo for helpful discussions.

* vanessa.kegler@unir.br

† igor.oliveira@ufla.br

‡ dominique@iftm.edu.br

§ rwnunes@fisica.ufmg.br

¶ teldo@fisica.ufmt.br

** erika.lima@fisica.ufmt.br

¹ K. S. Novoselov, F. Schedin, D. Jiang, T. J. Booth, V. V. Khotkevich, S. V. Morozov, and A. K. Geim, “Two-dimensional atomic crystals,” *Proceedings of the National Academy of Sciences* **102**, 10451 (2005).

² K. S. Novoselov, A. K. Geim, S. V. Morozov, D. Jiang, Y. Zhang, S. V. Dubonos, I. V. Grigorieva, and A. A. Firsov, “Electric field effect in atomically thin carbon films,” *Science* **306**, 666 (2004).

³ A. K. Geim and K. S. Novoselov, “The rise of graphene,” *Nature Materials* **6**, 183 (2007).

⁴ Bo Liu and Kun Zhou, “Recent progress on graphene-analogous 2d nanomaterials: Properties, modeling and applications,” *Progress in Materials Science* **100**, 99–169 (2019).

⁵ Seymour Cahangirov, Mehmet Topsakal, Ethem Aktürk, Hasan Şahin, and Salim Ciraci, “Two-and one-dimensional honeycomb structures of silicon and germanium,” *Physical review letters* **102**, 236804 (2009).

⁶ Cheng-Cheng Liu, Wanxiang Feng, and Yugui Yao, “Quantum spin hall effect in silicene and two-dimensional germanium,” *Physical review letters* **107**, 076802 (2011).

⁷ Lars Matthes, Olivia Pulci, and Friedhelm Bechstedt, “Massive dirac quasiparticles in the optical absorbance of graphene, silicene, germanene, and tinene,” *Journal of Physics: Condensed Matter* **25**, 395305 (2013).

⁸ Peizhe Tang, Pengcheng Chen, Wendong Cao, Huaqing Huang, Seymour Cahangirov, Lede Xian, Yong Xu, Shou-Cheng Zhang, Wenhui Duan, and Angel Rubio, “Stable two-dimensional dumbbell stanene: A quantum spin hall insulator,” *Physical Review B* **90**, 121408 (2014).

⁹ Feng-feng Zhu, Wei-jiong Chen, Yong Xu, Chun-lei Gao, Dan-dan Guan, Can-hua Liu, Dong Qian, Shou-Cheng Zhang, and Jin-feng Jia, “Epitaxial growth of two-dimensional stanene,” *Nature materials* **14**, 1020–1025 (2015).

¹⁰ Cheng-Cheng Liu, Wanxiang Feng, and Yugui Yao, “Quantum spin hall effect in silicene and two-dimensional germanium,” *Physical review letters* **107**, 076802 (2011).

¹¹ Bas Van den Broek, Michel Houssa, Emilio Scalise, Geof-

frey Pourtois, VV Afanas'ev, and Andre Stesmans, “Two-dimensional hexagonal tin: ab initio geometry, stability, electronic structure and functionalization,” *2D Materials* **1**, 021004 (2014).

¹² Frank Schwierz, “Graphene transistors,” *Nature nanotechnology* **5**, 487–496 (2010).

¹³ Jun Kang, Zhongming Wei, and Jingbo Li, “Graphyne and its family: recent theoretical advances,” *ACS applied materials & interfaces* **11**, 2692–2706 (2018).

¹⁴ Yongjun Li, Liang Xu, Huibiao Liu, and Yuliang Li, “Graphdiyne and graphyne: from theoretical predictions to practical construction,” *Chemical Society Reviews* **43**, 2572–2586 (2014).

¹⁵ Qitang Fan, Linghao Yan, Matthias W Tripp, Ondřej Krejčí, Stavrina Dimosthenous, Stefan R Kachel, Mengyi Chen, Adam S Foster, Ulrich Koert, Peter Liljeroth, *et al.*, “Biphenylene network: A nonbenzenoid carbon allotrope,” *Science* **372**, 852–856 (2021).

¹⁶ Andrey N Enyashin and Alexander L Ivanovskii, “Graphene allotropes,” *physica status solidi (b)* **248**, 1879–1883 (2011).

¹⁷ Susmita Jana, Arka Bandyopadhyay, Sujoy Datta, Debaprem Bhattacharya, and Debnarayan Jana, “Emerging properties of carbon based 2d material beyond graphene,” *Journal of Physics: Condensed Matter* **34**, 053001 (2021).

¹⁸ Paolo Bollella, Giovanni Fusco, Cristina Tortolini, Gabriella Sanzò, Gabriele Favero, Lo Gorton, and Riccarda Antiochia, “Beyond graphene: Electrochemical sensors and biosensors for biomarkers detection,” *Biosensors and Bioelectronics* **89**, 152–166 (2017).

¹⁹ Qing Peng, Albert K Dearden, Jared Crean, Liang Han, Sheng Liu, Xiaodong Wen, and Suvranu De, “New materials graphyne, graphdiyne, graphone, and graphane: review of properties, synthesis, and application in nanotechnology,” *Nanotechnology, science and applications* , 1–29 (2014).

²⁰ Yuanyuan Zhang, Zaizhen Zhang, Mohammed Ahmed Mustafa, Shelesh Krishna Saraswat, Shereen M Mekkey, Laith Yassen Qassem, Manal Morad Karim, Ayat H Athab, and Yasser Elmasry, “Application of biphenylene nanosheets for metronidazole detection,” *Journal of Molecular Liquids* **398**, 124216 (2024).

²¹ Jayeeta Lahiri, You Lin, Pinar Bozkurt, Ivan I Oleynik, and Matthias Batzill, “An extended defect in graphene as a metallic wire,” *Nature nanotechnology* **5**, 326–329 (2010).

- ²² Mahesh Datt Bhatt, Heeju Kim, and Gunn Kim, “Various defects in graphene: a review,” *RSC advances* **12**, 21520–21547 (2022).
- ²³ Cong Su, Hua Jiang, and Ji Feng, “Two-dimensional carbon allotrope with strong electronic anisotropy,” *Physical Review B—Condensed Matter and Materials Physics* **87**, 075453 (2013).
- ²⁴ Erika N Lima, Tome M Schmidt, and Ricardo W Nunes, “Topologically protected metallic states induced by a one-dimensional extended defect in the bulk of a 2d topological insulator,” *Nano Letters* **16**, 4025–4031 (2016).
- ²⁵ Erika N Lima, Tome M Schmidt, and R W Nunes, “Structural and topological phase transitions induced by strain in two-dimensional bismuth,” *Journal of Physics: Condensed Matter* **31**, 475001 (2019).
- ²⁶ Andreia Luisa da Rosa, Renato Borges Pontes, Erika Nascimento Lima, and Thomas Frauenheim, “New pentaocite phase of group-v nanostructures,” *physica status solidi (b)* **258**, 2100112 (2021).
- ²⁷ P. Hohenberg and W. Kohn, “Inhomogeneous electron gas,” *Phys. Rev.* **136**, B864–B871 (1964).
- ²⁸ W. Kohn and L. J. Sham, “Self-consistent equations including exchange and correlation effects,” *Phys. Rev.* **140**, A1133–A1138 (1965).
- ²⁹ G. Kresse and J. Furthmüller, “Efficient iterative schemes for ab initio total-energy calculations using a plane-wave basis set,” *Phys. Rev. B* **54**, 11169–11186 (1996).
- ³⁰ John P. Perdew, Kieron Burke, and Matthias Ernzerhof, “Generalized gradient approximation made simple,” *Phys. Rev. Lett.* **77**, 3865–3868 (1996).
- ³¹ John P. Perdew, Kieron Burke, and Matthias Ernzerhof, “Generalized gradient approximation made simple,” *Phys. Rev. Lett.* **77**, 3865–3868 (1996).
- ³² G. Kresse and D. Joubert, “From ultrasoft pseudopotentials to the projector augmented-wave method,” *Phys. Rev. B* **59**, 1758–1775 (1999).
- ³³ Hendrik J. Monkhorst and James D. Pack, “Special points for brillouin-zone integrations,” *Phys. Rev. B* **13**, 5188–5192 (1976).
- ³⁴ Atsushi Togo and Isao Tanaka, “First principles phonon calculations in materials science,” *Scripta Materialia* **108**, 1–5 (2015).
- ³⁵ Hans C Andersen, “Molecular dynamics simulations at constant pressure and/or temperature,” *The Journal of chemical physics* **72**, 2384–2393 (1980).
- ³⁶ Vei Wang, Nan Xu, Jin-Cheng Liu, Gang Tang, and Wen-Tong Geng, “Vaspkit: A user-friendly interface facilitating high-throughput computing and analysis using vasp code,” *Computer Physics Communications* **267**, 108033 (2021).
- ³⁷ Aliaksandr V Krukau, Oleg A Vydrov, Artur F Izmaylov, and Gustavo E Scuseria, “Influence of the exchange screening parameter on the performance of screened hybrid functionals,” *The Journal of chemical physics* **125** (2006).
- ³⁸ Kyozauro Takeda and Kenji Shiraishi, “Theoretical possibility of stage corrugation in si and ge analogs of graphite,” *Physical Review B* **50**, 14916 (1994).
- ³⁹ Feng-feng Zhu, Wei-jiong Chen, Yong Xu, Chun-lei Gao, Dan-dan Guan, Can-hua Liu, Dong Qian, Shou-Cheng Zhang, and Jin-feng Jia, “Epitaxial growth of two-dimensional stanene,” *Nature materials* **14**, 1020–1025 (2015).
- ⁴⁰ Qitang Fan, Linghao Yan, Matthias W. Tripp, Ondřej Krejčí, Stavrina Dimosthenous, Stefan R. Kachel, Mengyi Chen, Adam S. Foster, Ulrich Koert, Peter Liljeroth, and J. Michael Gottfried, “Biphenylene network: A nonbenzenoid carbon allotrope,” *Science* **372**, 852–856 (2021).
- ⁴¹ Max Born, “On the stability of crystal lattices. i,” in *Mathematical Proceedings of the Cambridge Philosophical Society*, Vol. 36 (Cambridge University Press, 1940) pp. 160–172.
- ⁴² Max Born and Kun Huang, *Dynamical theory of crystal lattices* (Oxford university press, 1996).
- ⁴³ Yujie Liao, XiZhi Shi, Tao Ouyang, Jin Li, Chunxiao Zhang, Chao Tang, Chaoyu He, and Jianxin Zhong, “New two-dimensional wide band gap hydrocarbon insulator by hydrogenation of a biphenylene sheet,” *The Journal of Physical Chemistry Letters* **12**, 8889–8896 (2021).
- ⁴⁴ Rita John and Benita Merlin, “Theoretical investigation of structural, electronic, and mechanical properties of two dimensional c, si, ge, sn,” *Crystal Structure Theory and Applications* **5**, 43–55 (2016).
- ⁴⁵ Yi Luo, Chongdan Ren, Yujing Xu, Jin Yu, Sake Wang, and Minglei Sun, “A first principles investigation on the structural, mechanical, electronic, and catalytic properties of biphenylene,” *Scientific reports* **11**, 19008 (2021).
- ⁴⁶ Qing Peng and Suvranu De, “Outstanding mechanical properties of monolayer mos 2 and its application in elastic energy storage,” *Physical Chemistry Chemical Physics* **15**, 19427–19437 (2013).
- ⁴⁷ Jin Tao, Wanfu Shen, Sen Wu, Lu Liu, Zhihong Feng, Chao Wang, Chunguang Hu, Pei Yao, Hao Zhang, Wei Pang, *et al.*, “Mechanical and electrical anisotropy of few-layer black phosphorus,” *ACS nano* **9**, 11362–11370 (2015).
- ⁴⁸ Yong Xu, Binghai Yan, Hai-Jun Zhang, Jing Wang, Gang Xu, Peizhe Tang, Wenhui Duan, and Shou-Cheng Zhang, “Large-gap quantum spin hall insulators in tin films,” *Physical review letters* **111**, 136804 (2013).
- ⁴⁹ Masae Takahashi, “Flat building blocks for flat silicene,” *Scientific Reports* **7**, 10855 (2017).
- ⁵⁰ Raad Chegel and Somayeh Behzad, “Tunable electronic, optical, and thermal properties of two-dimensional germanene via an external electric field,” *Scientific Reports* **10**, 704 (2020).
- ⁵¹ George W Crabtree and Mildred S Dresselhaus, “The hydrogen fuel alternative,” *Mrs Bulletin* **33**, 421–428 (2008).
- ⁵² John O Abe, API Popoola, Emmanuel Ajenifuja, and Olawale M Popoola, “Hydrogen energy, economy and storage: Review and recommendation,” *International journal of hydrogen energy* **44**, 15072–15086 (2019).
- ⁵³ Thanh Tuan Le, Prabhakar Sharma, Bhaskor Jyoti Bora, Viet Dung Tran, Thanh Hai Truong, Huu Cuong Le, and Phuoc Quy Phong Nguyen, “Fueling the future: A comprehensive review of hydrogen energy systems and their challenges,” *International Journal of Hydrogen Energy* (2023).
- ⁵⁴ Andrzej Lasia, “Mechanism and kinetics of the hydrogen evolution reaction,” *international journal of hydrogen energy* **44**, 19484–19518 (2019).
- ⁵⁵ Naiwrit Karmodak and Oliviero Andreussi, “Catalytic activity and stability of two-dimensional materials for the hydrogen evolution reaction,” *ACS Energy Letters* **5**, 885–891 (2020).
- ⁵⁶ Saisai Li, Jianrui Sun, and Jingqi Guan, “Strategies to improve electrocatalytic and photocatalytic performance of two-dimensional materials for hydrogen evolution reaction,” *Chinese Journal of Catalysis* **42**, 511–556 (2021).
- ⁵⁷ Jens Kehlet Nørskov, Thomas Bligaard, Ashildur Logadottir, JR Kitchin, Jingguang G Chen, S Pandalov, and U Stimming, “Trends in the exchange current for hydrogen

- evolution,” *Journal of The Electrochemical Society* **152**, J23 (2005).
- ⁵⁸ Yanan Zhou, Guoping Gao, Yan Li, Wei Chu, and Lin-Wang Wang, “Transition-metal single atoms in nitrogen-doped graphenes as efficient active centers for water splitting: a theoretical study,” *Physical Chemistry Chemical Physics* **21**, 3024–3032 (2019).
 - ⁵⁹ Mihir Ranjan Sahoo, Avijeet Ray, Rajeev Ahuja, and Nirpendra Singh, “Activation of metal-free porous basal plane of biphenylene through defects engineering for hydrogen evolution reaction,” *International Journal of Hydrogen Energy* **48**, 10545–10554 (2023).
 - ⁶⁰ Yuanju Qu, Ye Ke, Yangfan Shao, Wenzhou Chen, Chi Tat Kwok, Xingqiang Shi, and Hui Pan, “Effect of curvature on the hydrogen evolution reaction of graphene,” *The Journal of Physical Chemistry C* **122**, 25331–25338 (2018).
 - ⁶¹ Muhammad Sajjad, Surabhi Suresh Nair, Yarjan Abdul Samad, and Nirpendra Singh, “Colossal figure of merit and compelling her catalytic activity of holey graphyne,” *Scientific Reports* **13**, 9123 (2023).
 - ⁶² Yuanju Qu, Hui Pan, Chi Tat Kwok, and Zisheng Wang, “A first-principles study on the hydrogen evolution reaction of vs 2 nanoribbons,” *Physical Chemistry Chemical Physics* **17**, 24820–24825 (2015).
 - ⁶³ Hao-Ran Zhu, Yan-Ling Hu, Shi-Hao Wei, and Da-Yin Hua, “Single-metal atom anchored on boron monolayer (β 12) as an electrocatalyst for nitrogen reduction into ammonia at ambient conditions: a first-principles study,” *The Journal of Physical Chemistry C* **123**, 4274–4281 (2019).
 - ⁶⁴ Bo Zhang, Xiuli Fu, Li Song, and Xiaojun Wu, “Improving hydrogen evolution reaction performance by combining ditungsten carbide and nitrogen-doped graphene: A first-principles study,” *Carbon* **172**, 122–131 (2021).
 - ⁶⁵ Jingwei Liu, Guangtao Yu, Xuri Huang, and Wei Chen, “The crucial role of strained ring in enhancing the hydrogen evolution catalytic activity for the 2d carbon allotropes: a high-throughput first-principles investigation,” *2D Materials* **7**, 015015 (2019).
 - ⁶⁶ Yongqing Cai, Junfeng Gao, Shuai Chen, Qingqing Ke, Gang Zhang, and Yong-Wei Zhang, “Design of phosphorene for hydrogen evolution performance comparable to platinum,” *Chemistry of Materials* **31**, 8948–8956 (2019).
 - ⁶⁷ Ye Tian, Rui Mei, Da-zhong Xue, Xiao Zhang, and Wei Peng, “Enhanced electrocatalytic hydrogen evolution in graphene via defect engineering and heteroatoms co-doping,” *Electrochimica Acta* **219**, 781–789 (2016).
 - ⁶⁸ Lei Wang, Zhenhua Zeng, Wenpei Gao, Tristan Maxson, David Raciti, Michael Giroux, Xiaoqing Pan, Chao Wang, and Jeffrey Greeley, “Tunable intrinsic strain in two-dimensional transition metal electrocatalysts,” *Science* **363**, 870–874 (2019).
 - ⁶⁹ Sheng Chen, Hongyang Su, Youcheng Wang, Wenlong Wu, and Jie Zeng, “Size-controlled synthesis of platinum–copper hierarchical trigonal bipyramidal nanoframes,” *Angewandte Chemie* **127**, 110–115 (2015).
 - ⁷⁰ Jun Gu, Guangxu Lan, Yingying Jiang, Yanshuang Xu, Wei Zhu, Chuanhong Jin, and Yawen Zhang, “Shaped pt-ni nanocrystals with an ultrathin pt-enriched shell derived from one-pot hydrothermal synthesis as active electrocatalysts for oxygen reduction,” *Nano Research* **8**, 1480–1496 (2015).
 - ⁷¹ Ji-Eun Lee, Yu Jin Jang, Wenqian Xu, Zhenxing Feng, Hee-Young Park, Jin Young Kim, and Dong Ha Kim, “Ptfe nanoparticles supported on electroactive au–pani core@ shell nanoparticles for high performance bifunctional electrocatalysis,” *Journal of Materials Chemistry A* **5**, 13692–13699 (2017).
 - ⁷² Rajib Paul, Lin Zhu, Hao Chen, Jia Qu, and Liming Dai, “Recent advances in carbon-based metal-free electrocatalysts,” *Advanced Materials* **31**, 1806403 (2019).
 - ⁷³ Changqing Li and Jong-Beom Baek, “Recent advances in noble metal (pt, ru, and ir)-based electrocatalysts for efficient hydrogen evolution reaction,” *ACS omega* **5**, 31–40 (2019).